

# 2

## Abundance of elements in Ba stars I: Data Reduction & Stellar Atmospheric Parameters

### **2.1 Introduction**

Spectroscopy is the science of interaction between light and matter. It is one of the most powerful scientific tools to study the properties of distant stars and Galaxies. It can reveal,

not only the intrinsic properties of stars like chemical composition, temperature, density, mass, luminosity of a star, etc. but also some of the extrinsic parameters like distance, relative motion of the stars as well. A star can be assumed to be a black body and hence in principle can emit radiations at all possible wavelengths in the electromagnetic spectrum. Based on the wavelength range, astronomical spectroscopy can be divided into many branches: UV, optical, IR, radio and X-ray spectroscopy. Using different branches of its different aspects of a star can be studied. Here in our work we have the samples observed in the optical part of the spectrum. In this chapter, we shall describe the high resolution spectroscopic observations, data reduction procedures, the computational methods and analysis techniques involved in the study of spectra for finding the stellar atmospheric parameters.

## **2.2 Astronomical techniques**

In modern days reflecting telescopes are used to collect the radiant energy from distant objects which are then focused to a detector and then calibrated to get the spectral response. Next imagers are used to analyse the spatial distribution of photons from the source along with photometers which measure the number of photons collected from the source. Next with the help of a spectrograph the wavelength distribution of light can be understood. However, accurate pointing and timing are required to have a correlation of observations as different instruments could be working in different wavelength intervals located at different places. But for our analysis, understanding mainly the spectrograph is important since we are dealing with a wavelength distribution of light. A general discussion on the basics of an astronomical spectrograph can be found in (Drisya (2015)[143]).

### 2.2.1 Factors affecting the stars' spectrum

The possibility of light getting modified at the time of detection can't be overlooked not only because it has travelled a long distance through space but also it has travelled through the earth's atmosphere. However, there are some other reasons too

**Sky background:** The sky generally behaves as a noisy background to the light received from astronomical objects which occasionally makes the detection of faint targets extremely difficult(Drisya (2015)[143]).

**Atmospheric extinction:** The dimming of an images obtained by the telescopes can also result due to scattering as atmosphere contains dust and molecules. However, the amount of this dimming depends upon the altitude of the object and the local conditions of the atmosphere present at the time of observation(Drisya (2015)[143]).

**Transparency variations or Atmospheric scintillation:** As the wind blows the clouds across the field of view of the telescope therefore clouds too have an impact on the quality of the image. They can cause large variation ranging from partial attenuation due to the thin cloud to complete loss due to thick cloud (Drisya (2015)[143]). Basically it is the noise due to the earth's turbulent atmosphere which can be a dominant noise source in high-precision astronomical photometry when observing bright targets from the ground. This scintillation, which induces photometric variations in the range of  $\sim 0.1\%$  to  $1.0\%$ , limits the detection capabilities of ground based telescopes (Osborn et al. (2015)[144])

**Air Mass:** The air mass is defined as the quantity of air seen in the direction of the zenith ( $z$ ) along the line of sight. It is measure of the path length for light from a celestial source that passes through the atmosphere. Mathematically it is defined as

$$Air\ mass = \frac{\int_{h_0}^{h_1} \rho(z) \sec[h(z)] dh}{\int_{h_0}^{h_1} \rho(h) dh}$$

where  $h_0$  = altitude of the observing site,  $h_1$  = upper level of the atmosphere and  $\rho(h)$  = atmospheric density. At any particular wavelength,  $\lambda$ , we can relate  $m_0(\lambda)$ , the magnitude of the observed object outside the atmosphere, to  $m(\lambda)$ , the magnitude of the observed object at the surface of the earth, by  $m(\lambda) = m_0(\lambda) + \kappa(\lambda) X(z)$  where  $X(z)$  is the air mass,  $\kappa(\lambda)$  is the extinction coefficient at wavelength  $\lambda$  and  $z$  is the zenith distance (the angular distance of the object from the zenith at the time of observation). For small zenith angles  $X = \sec z$  is a reasonable approximation, but as  $z$  increases, refraction effects, curvature of the atmosphere and variations of air density with height can become important and the expression for  $X$  can be written as (Sterken and Manford (1992)[145])

$$X = \sec z - 0.0018167 - (\sec z - 1) - 0.002875(\sec z - 1)^2 - 0.0008083(\sec z - 1)^3.$$

**Seeing:** The blurring of images due to turbulence in the atmosphere is called as atmospheric seeing. The refractive index of atmosphere varies from layer to layer. Due to this some rays of light coming from the stars bend more than some others and thus the images get blurred which can in turn change the brightness of the stars too (Drisya (2015)[143]).

## 2.3 Observation

### 2.3.1 High resolution spectroscopy

The objects are selected from the Barium star (hereafter Ba star) catalogue of (Lü 1991[146]) and the spectra are taken from the ELODIE archive (Moultaka et al. (2004)[147]). The catalogue consists of 389 Ba stars. We have considered only those Ba stars for which high resolution spectra are available with S/N ratio  $\geq 10$  at  $5500\text{\AA}$ . The spectra recorded in a single exposure as 67 orders on a 1K CCD have a resolution of  $R \sim 42000$ . In our work the wavelength range spans from 4000 to  $6800\text{\AA}$ . The details are given as the following

#### Observatoire de Haute Provence (OHP)

The Observatoire de Haute-Provence (OHP) has a geographical co-ordinate bearing latitude

44<sup>0</sup>N and longitude 5.7<sup>0</sup>E and at an altitude of 650 meters in southeast of France. ELODIE is a cross-dispersed Echelle spectrograph used at the 1.93 m telescope of OHP which is mainly used for detection of extra solar planet and also for high resolution spectroscopic study of relatively bright astronomical objects. Baranne et al. (1996)[148] have given the details about the spectrograph and reduction procedures. In one single exposure a spectrum at a resolution  $(\frac{\lambda}{d\lambda}) \sim 42000$  ranging from 3906 – 6811 Å is recorded on a 1024 × 1024 CCD, which is achieved by using a  $\tan\theta = 4$  Echelle grating and a combination of a prism and a grism as cross-disperser. An automatic on-line data reduction technique called TACOS reduces the ELODIE echelle spectra, ie optimal extraction, just after the exposures. The shape of the orders are relatively stable on the CCD as they find the application of fibres to feed the spectrograph. All the images coming from the spectrograph are saved on a disk for security purposes. Then the CCD frames are processed for correction of bad pixels, offset and dark current subtraction, etc. After the extraction Wavelength calibrations are done using Thorium lamps. And lastly all the data taken with Elodie spectrograph are deposited in the ELODIE archive.

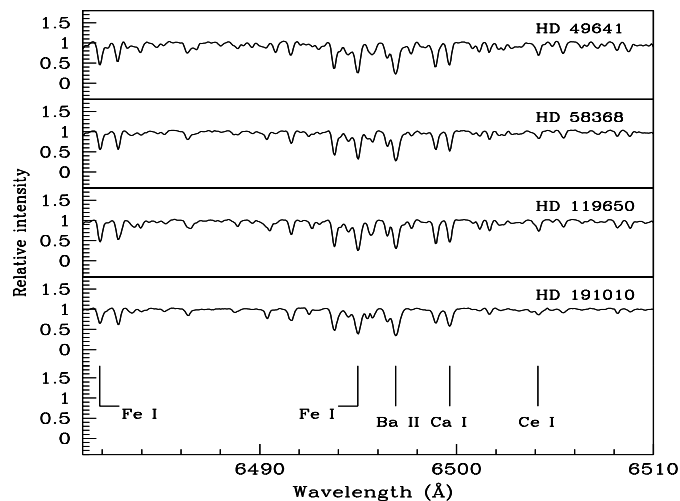


Fig. 2.1 Sample spectra of a few programme stars in the wavelength region 6480 – 6510 Å.

## 2.4 Data Reduction

This section describes the standard procedures for the extraction of CCD data with IRAF (Image Reduction and Analysis Facility) which is owned by the National Optical Astronomy Observatories (NOAO). IRAF provides a wide range of image processing tools by which one can process a raw two dimensional data into a one dimensional data for analysis. We have trimmed the section into an area which contains only useful data. Then zero correction and flat field correction are done for the reduction of the CCD data using CCDPROC task from CCDRED package. The Bias frames or Zero frames, which are taken with zero exposure time for correcting the zero of the CCD are then combined to a master bias using the ZERO COMBINE task in IRAF which needs to be subtracted from all the other frames for zero correction. Then dark current which arises due to heat has also been removed by using the dark exposures. However, for CCDs which are cryogenically cooled to liquid nitrogen temperature ( $-77$  K) this correction is not needed. Then flat frames, which are nothing but calibrating frames with a uniform source like halogen lamps are used to remove the pixel to pixel variations of the light sensitivity of the CCDs. Many flat frames were taken to improve the quality and then combined them into a master flat. Then this master flat is then normalised and by dividing the object frames by the normalised master flat helps to reduce the multiplicative error in the data. These steps are done using the tasks FLAT COMBINE and RESPONSE in IRAF. Next, the spectra (as counts vs pixels) has been extracted using APALL in apextract converted into wavelengths by using an arc spectrum along with the bias subtracted arc frame. The spectral lines in the arc spectrum are identified using the task IDENTIFY (for single order spectra) or ECIDENTIFY (for Echelle spectra) with the help of available identification charts. Then these arc frames are given as the reference to the object frames for the wavelength calibration using the task REFSPEC. The wavelength calibrated images are then corrected for dispersion using the task DISPCOR and continuum fitted for the further analysis.

## 2.5 Data Analysis

With the advent of powerful data processing and analysis techniques, which continues to evolve, the astronomical community has become very sophisticated in setting requirements and figures of merit for the technical capabilities for any observation. We too, in order to get a detailed abundance analysis and the physical conditions of a star, the effective temperature ( $T_{eff}$ ) and surface gravity ( $\log g$ ), which have close connection with the mass ( $M$ ), radius ( $R$ ) and luminosity ( $L$ ) of a star, have found out. The following sections give the details of the important terms involved in the calculation of stellar atmospheric parameters.

### 2.5.1 Bolometric magnitude

The bolometric magnitude of a star is a measure of the total radiation of a star emitted across all wavelengths of the electromagnetic spectrum. We measure the energy radiated by a using a detector placed on earth. Very cool and very hot objects emit radiations at far infrared and ultraviolet regions respectively, which can't be detected from earth. Hence corrections need to be applied to the absolute magnitudes of the stellar objects to find the bolometric magnitudes which are large for both very cool and very hot stars, but are relatively small for stars like the Sun (Drisy (2015)[143]). The absolute magnitude ( $M$ ) and bolometric magnitude are related by the following expression

$$M_{bol} = M - (5 \log d + 5) + BC \quad (2.1)$$

where  $d$  (distance in parsec) =  $1/p$ ,  $p$  is the parallax angle in arcsec,  $BC$  is the bolometric correction of the star.

## 2.5.2 Luminosity

The luminosity  $L$  of a star is the total energy output of the star per unit time. The bolometric magnitude of a star in comparison to the sun are to the normalised luminosities via Pogson's equation as

$$M_{bol\odot} - M_{bol} = 2.5 \log \frac{L}{L_{\odot}} \quad (2.2)$$

## 2.5.3 Stellar Masses

Dredge-up mechanisms, mass loss episodes, convective overshooting and updated opacities have been considered for estimating the masses of the sample stars by using their positions in the H-R diagram using the evolutionary tracks given by Girardi et al. (2000)[149]. These evolutionary tracks start from Zero age main-sequence and end either at thermally pulsing AGB stage or carbon ignition with initial masses ranging from  $0.6M_{\odot}$  to  $120M_{\odot}$  and different initial compositions with  $Y(\text{He mass fraction}) = 0.273$  and  $Z = 0.019$  etc., where  $Z$  is the global metallicity for all the other metals as in our case.

## 2.5.4 Effective temperature

Effective temperature may be defined as the temperature of an equivalent black body that gives the same total power per unit area thus in other words it is the total radiant power per unit area, at stellar surface and thus, it is directly related to stellar luminosity and radius. By Stephan's law

$$\sigma T_{eff}^4 = \int F_V dV = \frac{L}{4\pi R^2} \quad (2.3)$$

where  $R$  is the radius is taken as the depth of formation of the continuum, which, in the visible region is approximately constant for most stars (Gray (1992)[150])

### 2.5.5 Surface gravity

Surface gravity ( $g$ ) of an object is the acceleration due to gravity on the surface of the object which is responsible for the pressure resulted in the stellar surface. Logarithmically, in solar units the surface gravity can be written as (Drisya (2015)[143])

$$\log g = \log M - 2 \log R + 4.437 \quad (2.4)$$

which is directly related to mass  $M$  and radius  $R$  of the object. A star with higher mass, but lower radius will be denser and also have higher pressure. A higher pressure will lead to a larger number of atoms per unit area leading to a stronger spectral line, which in turn results in a decrease of ionic line strength since more and more free electrons will get chance to combine with ions as the density is going to be very high.

### 2.5.6 Micro-turbulence

Micro-turbulence is the small scale motions of particles/atoms moving in random directions with a Maxwellian distribution of speeds in the photosphere which is treated like an additional thermal velocity in the region of spectral line formation. The size of the turbulent cells is very small compared with the optical depth and the cells of gas whose distribution of velocity components can be thought as gaussian(Drisya (2015)[143]). It has a peculiar effect on the shape of a spectral line, because the motion of the atoms broadens spectral line profiles of elements without affecting the chemical abundance. This implies that the equivalent width of the line does not have any correlation with the abundances. The strength of the microturbulence (symbolized by  $\zeta$ , in units of  $\text{kms}^{-1}$ ) can be determined by comparing the broadening of strong lines versus weak lines.

### 2.5.7 Equivalent width

The equivalent width ( $W$ )(Fig. 2.2) is used to compare the strengths of different absorption lines from a source, or the same absorption line arising from several different sources and also as a quantitative measure of the strength of spectral features. The way to find the equivalent width of a spectral line is by considering a rectangle with a height equal to that of the continuum ie a rectangular box of the same area, extending from the continuum to the 0 flux line, and finding the width such that the area of the rectangle is equal to the area in the spectral line. Mathematically

$$W = \int \frac{F_c - F_\lambda}{F_c} d\lambda \quad (2.5)$$

where  $F_\lambda$  is the radiant flux and  $F_c$  is the continuum flux (Drisy (2015)[143]). Another measure of width of a spectral line is full width at half maximum (FWHM) where the width of a spectrum curve measured between those points on the flux-axis which are half the maximum amplitude. In our case we have measured the equivalent width of absorption lines in our programme stars spectra by fitting a Gaussian to the absorption lines.

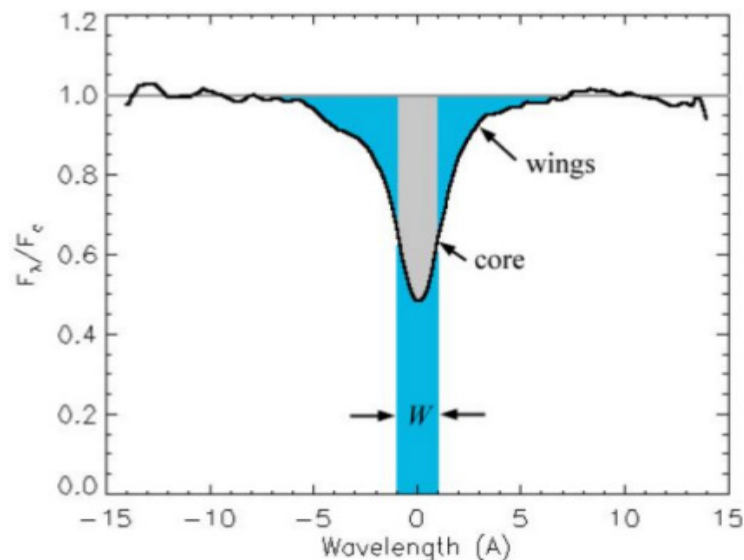


Fig. 2.2 The equivalent width of an absorption line.(Drisy (2015)[143])

### 2.5.8 Optical depth and opacity

When light travels through a medium, some photons get absorbed in the medium and the amount of absorption entirely depends upon the composition, density, temperature and the distance travelled by the light in the medium as well. If the absorption takes place at a wavelength  $\lambda$  which results in intensity decrement by an amount  $dI_\lambda$  then mathematically it can be written as (Drisya (2015)[143])

$$dI_\lambda = -K_\lambda \rho I_\lambda ds \quad (2.6)$$

where  $ds$  is the distance travelled and  $\rho$  is the density of the medium and the proportionality constant  $K$  is called the absorption coefficient or opacity which is defined as the cross-section for the absorbing photons of wavelength  $\lambda$  per unit mass of stellar material or it is the capacity of the material to absorb photons. Integrating the above equation within the limits  $s = 0$  to  $s = s$ , then  $I_\lambda$  is given by (Drisya (2015)[143])

$$I_\lambda = I_{\lambda,0} e^{-\int_0^s K_\lambda \rho ds} = I_{\lambda,0} e^{-K_\lambda \rho s} \quad (2.7)$$

where  $-K_\lambda \rho ds$  is called as optical depth  $d\tau_\lambda$  which obviously depends on the wavelength can be defined as number of mean free paths from the rays original position to the surface where the mean free path is  $l = \frac{1}{\kappa_\lambda \rho}$ . Thus the intensity of light declines exponentially by a factor of  $e^{-1}$  for this mean free path.

### 2.5.9 Model atmosphere

The chemical analysis of a spectrum is done by comparing the observed features with the theoretical predictions assuming a model atmosphere of the star. To construct the model photosphere few assumptions are made as following

1. Plane parallel geometry, making all physical variables a function of only one space coordinate.
2. Hydrostatic equilibrium, meaning that the photosphere is not undergoing large scale accelerations comparable to the surface gravity.
3. Structures such as starspots and granulations and magnetic fields are neglected.

The equation for hydrostatic equilibrium as given below are then solved to construct the model atmospheres (Drisya (2015)[143])

$$\frac{dF}{dA} = dP = \rho g dx$$

where  $\rho$  is the density,  $dA dx$  is the volume,  $g$  is the surface gravity and  $dP$  is the pressure. A model atmosphere consists of a table of numbers giving the pressure as a function of optical depth for an assumed chemical composition. Depending upon the purpose of usage some model contains intensity, absorption coefficient, electron pressure etc also. Usually photosphere is assumed to have seventy two layers and the model atmosphere contains seventy two rows each representing each layer of atmosphere. It is very difficult to establish a perfect thermodynamic equilibrium in stars. The temperature of the star varies with location. However, the thermodynamic equilibrium can be assumed in a small region of unit optical depth and is called the Local Thermodynamic Equilibrium (LTE). At LTE, photosphere can be represented by one temperature and optical depth. Also, only collisionally induced transition occurs at LTE.

### 2.5.10 Radial velocity estimation

Radial velocities of our programme stars are calculated using a selected set of clean unblended lines in the spectra using the equation

$$V_r = \frac{\lambda_{obs} - \lambda_{lab}}{\lambda_{lab}} \times c \quad (2.8)$$

where  $c$  is the vel. of light. Application of this formula requires laboratory measurements of the rest wavelength to a very high accuracy. When an object moves towards us, the transition is shifted to shorter wavelengths and it is called blue shifted. Similarly, when an object moves away from us the transition is towards a longer wavelengths and is called as redshifted.

### **Radial velocity of our programme stars:**

Radial velocities of the programme stars are calculated using a selected set of clean unblended lines in the spectra. Estimated mean radial velocities are presented in Table 2.1. The literature values are also presented for a comparison. Radial velocity variations are reported in Pourbaix et al. (2004)[175] for stars, HD-49641, HD-58368 and in Gontcharov (2006)[176] for HD-119650, HD-191010. Our radial velocity estimate for HD-119650 shows a small deviation of  $\sim 0.6 \text{ kms}^{-1}$  from the literature value in comparison to the rest three objects. However all objects are found to be low-velocity objects ( $V_r < 45 \text{ kms}^{-1}$ ). Object HD-49641 comes with enhanced heavy elements and radial velocity indicating a mass-transfer scenario similar to the ones that hold for CH stars and CEMP-s stars. Object HD-49641 heavy elements significantly enhanced together with the variations observed in radial velocity estimates, a mass-transfer scenario similar to the ones that hold for barium stars, CH stars and CEMP-s stars is likely for the origin of this object indicating its binarity. However significant enhancement in Eu abundance demands investigation of its formation scenario as well as to understand its abundance patterns. McClure (1983)[164] found HD-58368 to be a radial velocity variable with a variation of  $\sim \pm 12 \text{ kms}^{-1}$  indicating its binarity. A mass-transfer scenario is likely to hold for this object too. For the other two objects HD-119650, HD-191010 possession of radial velocity indicates their binarity and the observed abundance pattern suggested a mass-transfer might have operated in these two barium stars too.

### 2.5.11 Photometric temperature estimation

The effective temperature of an object can be derived directly from the angular diameter and bolometric fluxes of a star. But this direct method finds very limited applicability. However an indirect method was developed by Alonso et al. (1996)[151] to determine the temperatures of stellar dwarfs and sub-dwarfs, which can even be extended to main-sequence stars and giants, the method called as Infrared flux method. The infrared flux method uses the ratio between bolometric flux and monochromatic flux at the infrared wavelength of the continuum. This ratio is called observational R factor, which is then compared with the theoretically calculated  $R_{th}$  for which a theoretical model atmosphere developed by Kurucz (1991[152], 1993[153]) are used. Then monochromatic fluxes are determined observationally using IR photometry. The calibrations then relate  $T_{eff}$  with Stromgren indices, metallicity, [Fe/H] and color indices (V-B), (V-K), (J-H) and (J-K) which holds good within a temperature and metallicity range  $4000 \leq T_{eff} \leq 7000$  K and  $-2.5 \leq [Fe/H] \leq 0$ . However Alonso et al. (1996)[151] calibrations use Johnson photometric systems for UBVRI and use TCS (Telescopio Carlos Sanchez) system for IR colours, (J-H) and (J-K). Here we have used colour-temperature calibrations of Alonso et al. (1996)[151] that relate  $T_{eff}$  with various optical and near-IR colours. The estimated uncertainty in the temperature calibrations is  $\sim 100$  K. Although the difference between 2MASS infrared photometric system and photometry data measured in the TCS system used by Alonso et al. (1996)[151] to derive the  $T_{eff}$  scales is very small, the necessary transformations between these photometric systems

Table 2.1 Radial velocities in  $\text{kms}^{-1}$  of programme stars.

Object	$V_r$ (our estimates)	S/N ratio at 5500 Å	Date of Observation	Time(UT) of Observation	$V_r$ , (literature values)	Ref.
HD49641	7.20	121	17.12.2000	02:06:02	4.45,	Pourbaix et al. (2004)[175]
HD58368	41.67	109	26.11.2001	03:57:22	37.81,	Pourbaix et al. (2004)[175]
HD119650	-5.10	143	23.5.2003	21:48:20	-5.70,	Gontcharov (2006)[176]
HD191010	20.60	149	29.7.2003	22:53:58	18.10,	Gontcharov (2006)[176]

are performed using transformation relations from Ramírez & Meléndez (2004)[154] and Alonso et al. (1996[151], 1999[155]). (V-K) is the preferred temperature indicator since both pass-bands are only marginally affected by the presence of the strong molecular lines in the temperature range of carbon stars. The B-V colour of a star with strong molecular carbon absorption features depends not only on  $T_{eff}$ , but also on the metallicity of the star and on the strength of its molecular carbon absorption features, due to the effect of CH molecular absorption in the B band. (B-V) colour often gives a much lower value than the actual surface temperature of the star due to the effect of CH molecular absorption in the B band. We have assumed that the effects of reddening on the measured colours are negligible. The equations used for the calculations are as follows (Karinkuzhi & Goswami 2014[156]).

$$J_{TCS} = J_{2MASS} + 0.001 - 0.049(J_{2MASS} - KJ_{2MASS})$$

$$H_{TCS} = H_{2MASS} - 0.018 + 0.003(J_{2MASS} - KJ_{2MASS})$$

$$K_{TCS} = K_{2MASS} - 0.014 + 0.034(J_{2MASS} - KJ_{2MASS})$$

$$K_J = K_{TCS} + 0.042 - 0.019 \left[ \frac{(J_{TCS} - K_{TCS}) - 0.008}{0.910} \right]$$

$$\Theta_{JK} = 0.582 + 0.799(J_{TCS} - K_{TCS}) + 0.085(J_{TCS} - K_{TCS})^2$$

$$(V - K)_{TCS} = 0.050 + 0.993(V - K_J)$$

$$\Theta_{JH} = 0.587 + 0.922(J_{TCS} - H_{TCS}) + 0.218(J_{TCS} - H_{TCS})^2$$

$$+ 0.016[Fe/H](J_{TCS} - H_{TCS})$$

$$\Theta_{VK} = 0.555 + 0.195(V - K)_{TCS} + 0.013(V - K)_{TCS}^2 - 0.008(V - K)_{TCS}[Fe/H]$$

$$+ 0.009[Fe/H] - 0.002[Fe/H]^2$$

$$\Theta_{BV}[Fe/H] = 0.541 + 0.533(B - V) + 0.007(B - V)^2 - 0.019(B - V)[Fe/H]$$

$$- 0.047[Fe/H] - 0.011[Fe/H]^2$$

where  $xy$  to be indicating J-K, J-H, V-K and B-V where magnitude (V) is in Johnson system.

Now the  $T_{eff}$  is calculated as

$$T_{eff(xy)} = \frac{5040}{\Theta_{xy}} \quad (2.9)$$

### Photometric temperatures of our programme star:

The basic data for these four stars listed in Table 2.2 are taken from the SIMBAD Database which is an astronomical database of objects beyond the Solar System. It is maintained by the Centre de données astronomiques de Strasbourg (CDS), France. The estimates of

Table 2.2 Basic data for the programme stars

Star ID	RA(2000)	Dec.(2000)	B	V	J	H	K
HD 49641	06 49 29.4495	+03 41 30.189	8.47	7.12	5.078	4.506	4.253
HD 58368	07 25 38.9681	+07 33 39.046	9.01	7.99	6.334	5.919	5.773
HD 119650	13 44 27.1157	+00 42 07.020	8.78	7.59	5.668	5.164	4.908
HD 191010	20 06 45.8410	+25 41 06.790	9.13	8.17	6.488	6.092	5.970

photometric temperatures at metallicity values from  $-0.5$  to  $-1.5$  for the objects presented in Table 2.4 are estimated using the colour temperature calibrations using the Table 2.3 (Alonso et al. (1999)[155]) with its erratum in Alonso et al. (2001)[174]. This calibration was derived by using a large number of lower main-sequence stars and subgiants, whose temperatures were measured by the infrared flux method, and holds within temperature and metallicity ranges of  $4000 \leq T_{eff}/K \leq 7000$  and  $-2.5 \leq [Fe/H] \leq 0$ .

$$\Theta_{eff} = a_0 + a_1X + a_2X^2 + a_3X[Fe/H] + a_4[Fe/H] + a_5[Fe/H]^2$$

where  $X$  is for the colour and the co-efficients  $a_i$  with  $i=1 \dots 5$  bears the following tabulated value. The numbers in the parenthesis below  $T_{eff}$  of Table 2.4 indicate the metallicity values

Table 2.3 Value of the co-efficients

color	$a_0$	$a_1$	$a_2$	$a_3$	$a_4$	$a_5$
B-V	0.6177	0.4354	$-4.025 \times 10^{-3}$	$5.204 \times 10^{-2}$	-0.1127	$-1.385 \times 10^{-2}$
V-K	0.3770	0.3660	$-3.170 \times 10^{-2}$	$-3.074 \times 10^{-3}$	$-2.765 \times 10^{-3}$	$-2.973 \times 10^{-3}$
J-H	0.5977	1.015	$-1.020 \times 10^{-1}$	$-1.029 \times 10^{-2}$	$3.006 \times 10^{-2}$	$1.013 \times 10^{-2}$
J-K	0.5816	0.9134	-0.1443	0.0000	0.0000	0.0000

at which the temperatures are calculated and  $T_{sp}$  is the spectroscopic estimate of the effective temperature. Temperatures are given in Kelvin.

Table 2.4 Temperatures from photometry

Star ID	$T_{eff}$ (J-K)	$T_{eff}$ (-0.5) (J-H)	$T_{eff}$ (-0.5) (V-K)	$T_{eff}$ (-1.0) (J-H)	$T_{eff}$ (-1.0) (V-K)	$T_{eff}$ (-1.5) (J-H)	$T_{eff}$ (-1.5) (V-K)	$T_{eff}$ (-0.5) (B-V)	$T_{eff}$ (-1.0) (B-V)	$T_{eff}$ (-1.5) (B-V)	$T_{sp}$
HD49641	4199	4526	4312	4544	4298	4534	4291	3919	3686	3497	4700
HD58368	4918	5135	4863	5163	4851	5154	4846	4433	4167	3953	5095
HD119650	4350	4779	4445	4802	4432	4792	4425	4152	3904	3703	4825
HD191010	5068	5219	4881	5248	4869	5240	4864	4541	4268	4049	5325

### 2.5.12 Stellar Atmospheric parameters

There is a direct correlation between the  $T_{eff}$  of a star with the excitation potential of a given atomic species. Or in other words, in general, the measurements of atomic lines with differing excitation potentials can be used to determine the effective temperature of a star. However the situation is different under LTE conditions where the abundances predicted from individual lines should not show any correlation to the excitation potential of the lines. In our work we have assumed LTE and We have used a set of FeI and FeII lines with excitation potential in the range 0.0 – 5.0 eV and equivalent width 20 mÅ to 190 mÅ to find the stellar atmospheric parameters. The  $T_{eff}$  is determined by making the slope of the abundance versus excitation potential of FeI lines to be nearly zero. The initial value of the temperature is taken from the photometric estimates and arrived at a final value by an iterative method with the slope nearly equal to zero. The micro-turbulent velocity was estimated at a given effective temperature by demanding that there be no dependence of the derived Fe I abundance on the equivalent

width of the corresponding lines. The surface gravity is fixed at a value that gives the same abundances for Fe I and Fe II lines. Clean Fe II lines are more difficult to detect than Fe I lines, so we were limited to 4 – 10 Fe II lines for the abundance analysis of our sample stars. The strength of a spectral line which depends on the number of atoms undergoing transition gives the abundance of the element involved in the transition.

### **Stellar Atmospheric parameters of our programme stars:**

A selected set of unblended Fe I and Fe II lines used for the present analysis to find the stellar atmospheric parameters are listed in Appendix A. The excitation potential of the lines are in the range 0.0 – 5.0 eV and equivalent width in the range 20 mÅ to 190 mÅ. We have assumed LTE for our calculations. An updated 2014 version of MOOG (Snedden (1973)[157]) was used for the calculations. Model atmospheres (available at <http://cfaku5.cfa.harvard.edu/> and labelled with a suffix *odfnew*) were selected from the Kurucz grid of model atmospheres with no convective overshooting. Solar abundances are taken from Asplund, Grevesse & Sauval (2009)[177]. The effective temperature is determined by making the slope of the abundance versus excitation potential of Fe I lines to be nearly zero. The initial value of temperature is taken from the photometric estimates and arrived at a final value by an iterative method with the slope nearly equal to zero (Fig. 2.3, left panel). The microturbulent velocity is estimated at a given effective temperature by demanding that there be no dependence of the derived Fe I abundance on the equivalent width of the corresponding lines (Fig. 2.3, right panel). The surface gravity is fixed at a value that gives same abundances for Fe I and Fe II lines. Clean Fe II lines are more difficult to find than Fe I lines. In most cases, we were limited to 4 to 10 Fe II lines for our analyses. Derived atmospheric parameters are listed in Table 2.5.

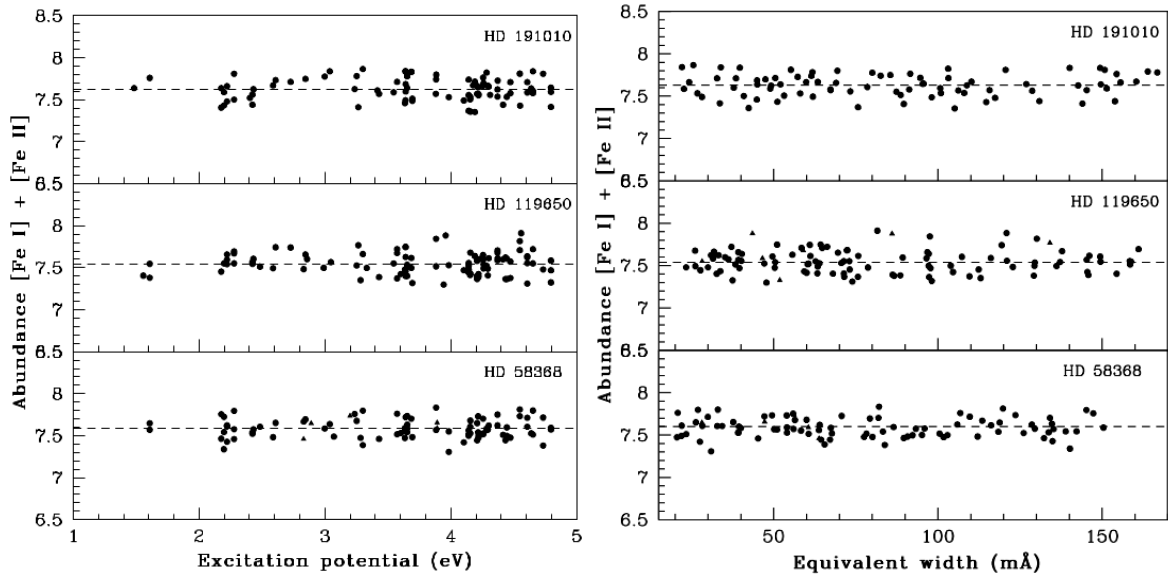


Fig. 2.3 Left panel: The Fe abundances (Fe I & Fe II) vs excitation potential, Right panel: The Fe abundances (Fe I & Fe II) vs equivalent width

Table 2.5 Derived atmospheric parameters for the programme stars.  $T_{eff}$  is in Kelvins and Micro-turbulent vel.  $\zeta$  is in  $\text{kms}^{-1}$

Star ID	$T_{eff}$	$\log g$	$\zeta$	[Fe I/H]	[Fe II/H]
HD 49641	4700	3.40	1.77	-0.05	-0.02
HD 58368	5095	3.45	1.37	0.09	0.12
HD 119650	4825	2.85	1.62	0.04	0.14
HD 191010	5325	2.38	1.92	0.13	0.12

### 2.5.13 Calculation of Elemental abundances

The methods used to determine the abundance of chemical elements in stellar atmospheres are based on the intensity of spectral lines. This is done by comparing the observed high resolution spectrum with a calculated spectrum. The results will of course entirely depend upon the model atmospheres and the line formation mechanisms. The methods used are

#### 1. Fine analysis method:

In this method the observed equivalent width is compared with the equivalent width calculated on the basis of a selected model photospheres. The equivalent width  $\leq 190 \text{ m}\text{\AA}$  are used as

in our case too so that NLTE effects do not get a chance to play a significant role along with the micro-turbulence and damping constants. However to get an accurate measurement of equivalent widths we need very high resolution spectra ( $R \geq 20000$ ) with a very high S/N ( $\geq 20$ ) ratio.

## 2. The spectrum synthesis method:

Spectrum synthesis method is generally applied to crowded regions with severe line blending. In this method deals with the comparison between an observed line profile with a theoretically computed profile instead of equivalent widths. All the line broadening mechanisms are taken care off for calculating the theoretical profiles. An extensive line list for each element at different ionisation states, known laboratory wavelengths,  $\log g$  and excitation potential are the pre-requisites for the accurate measurement of the abundances. Sometimes this method is also used as a tool to confirm the results obtained from the standard equivalent width method.

## MOOG:

MOOG is a FORTRAN code that uses LTE conditions developed by Sneden (1973[157]) for his PhD thesis and subsequently revised by him which is used to find the chemical abundances of stars. MOOG needs a model photosphere together with a list of atomic or molecular transitions as inputs for the analysis. The subroutine *abfind* performs a numerous iterations varying the abundances which finally yields the computed equivalent widths that agree with observed ones previously measured with other software packages with respect to a particular atmospheric model. For the synthesis, the program *synth* is used to fit the observed spectrum to the theoretically calculated spectrum. In this case also, a set of synthetic spectra are formed to match the observed one. The detailed description of these codes and methods can be found in Chris Sneden's thesis and in a review article by Castelli & Hack (1990)[158].

### 2.5.14 Hyperfine splitting and Elemental abundances

When the spin angular momentum of the nucleus interacts with the total angular momentum of the electrons, the splitting of energy level occurs. This will lead to transition between different levels and as a result of that width of a spectral line will broaden. Abundances are calculated using these spectral lines will lead to wrong assessment. Hence hyperfine correction needs to be incorporated during abundance analysis. We have synthesised the elements Sc, V, Mn, Ba, La and Eu considering the hyperfine splitting of levels and their contributions to the total abundances.

## 2.6 Error Analysis

The error in the equivalent width measurement is going to have an affect on the measurement of surface gravity and micro turbulent velocities which will in turn lead to inaccurate determination of atmospheric parameters. This will further direct to erroneous measurement of the elemental abundances. We have calculated the error in the in the atmospheric parameters results as described by Ryan et al. (1996)[81]. The abundances measured here using the spectrum synthesis method, the error is uniformly taken as 0.2 dex by considering the fitting error of 0.1 dex and error in log gf values as 0.1 dex. For the abundance of elements using a single line then the errors will be from the measurement of atmospheric parameters. In such cases minimum error has been found by considering the respective standard deviation of the iron abundances along with the uncertainties in temperature, micro-turbulent velocities and surface gravities which is approximately 0.1. We have assumed an error of 100 K in effective temperature corresponding to 0.1 dex in abundances. These values as typically accepted for the minimum error in giants and subgiants. When a large number of lines are used for the calculation of abundances, the standard deviation of the abundances derived using individual lines is taken as the error. Then the total minimum error is calculated using the following

equation (Drisya (2015)[143])

$$E_r = (E_{r1}^2 + E_{r2}^2 + E_{r3}^2 + E_{r4}^2 + \dots + E_{rn}^2)^{\frac{1}{2}} \quad (2.10)$$

### **Error Analysis of our programme stars:**

The errors in the elemental abundances are mainly due to the errors in deriving the atmospheric parameters which have contributions from the measurement of the equivalent widths of Fe lines. The minimum error in the elemental abundances are taken as the standard deviation of the Fe abundance derived for each objects. These are listed in Table 3.2. The minimum error in temperature is taken as  $\pm 100$  K and for  $\log g$  as  $\pm 0.1$  dex. We have calculated the errors in the atmospheric parameters as described by Ryan et al. (1996)[81]. In order to show the effect of temperature variations in the abundance pattern we have plotted the Fe abundances with respect to the excitation potential values at three different temperature values, the adopted temperature ( $T_{eff}$ ) and  $T_{eff} \pm 100$  K (Fig. 2.4, upper panel). In the middle plot of Fig. 2.4, upper panel, shows the abundances corresponding to the adopted  $T_{eff}$ . The upper and the lower plots of the same panel show the variation in the abundance trend due to the variation of  $T_{eff}$  by +100 and -100 K, respectively. Similarly, the effect on abundance trends due to variation in the adopted  $\log g$  values by  $\pm 0.1$  dex is also shown in Fig. 2.4 (lower panel). In the middle plot of (Fig. 2.4, lower panel) shows the abundances corresponding to the adopted  $\log g$ . In the same panel, the upper and the lower plots show the variation in the abundance trend due to the variation of  $\log g$  by +0.1 and -0.1, respectively. The errors presented in Tables 3.2 correspond to the standard errors when abundances are measured using more than one line. For abundances that are derived using a single line or by using spectrum synthesis calculations an error of  $\pm 0.2$  dex is considered. A change by an amount  $\pm 0.2$  dex from the adopted abundance is found to be necessary to notice a visual separation between the different synthesized plots.

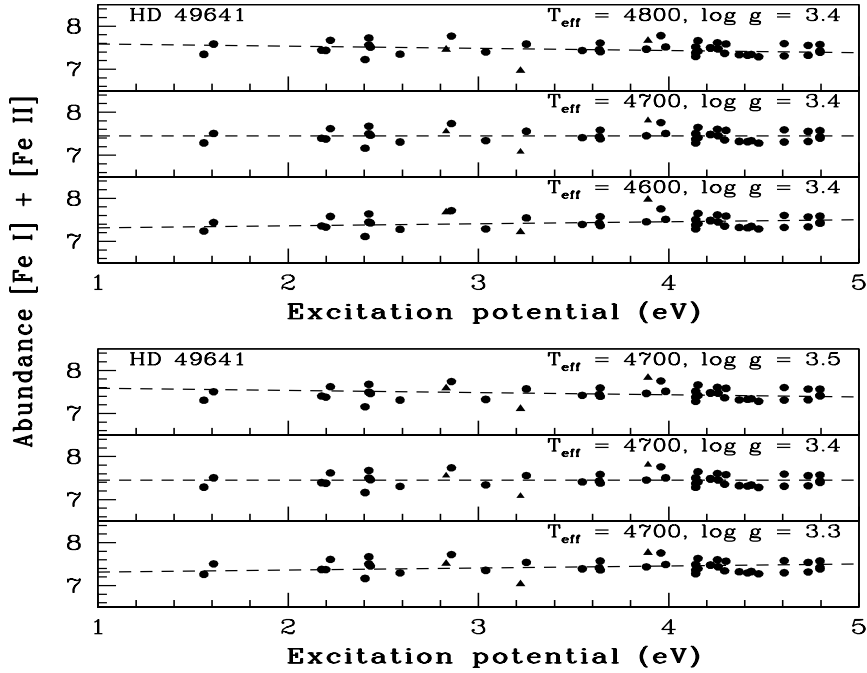


Fig. 2.4 The abundances of Fe I and Fe II lines as a function of excitation potential. The filled circles indicate Fe I lines and filled triangles indicate Fe II lines.

## 2.7 Summary

The tools for spectroscopic analysis of stars have been discussed and using those techniques we have estimated the stellar atmospheric parameters, the effective temperature  $T_{eff}$ , the surface gravity  $\log g$ , microturbulent velocity  $\zeta$  and metallicity  $[Fe/H]$  from local thermodynamic equilibrium analysis using model atmospheres. The high Resolution spectra ( $R \sim 42000$ ) of four chemically peculiar objects spanning a wavelength range from 4000 to 6800 Å, are taken from the ELODIE archive.